Dual Activity Lysophosphatidic Acid Receptor Pan-Antagonist/ Autotaxin Inhibitor Reduces Breast Cancer Cell Migration *In vitro* and Causes Tumor Regression *In vivo*

Honglu Zhang,[1] Xiaoyu Xu,[1] Joanna Gajewiak,[1] Ryoko Tsukahara,[2] Yuko Fujiwara,[2] Jianxiong Liu,[2] James I. Fells,[3] Donna Perygin,[3] Abby L. Parrill,[3] Gabor Tigyi,[2] and Glenn D. Prestwich[1]

[1]Department of Medicinal Chemistry, University of Utah, Salt Lake City, Utah; [2]Department of Physiology, University of Tennessee; [3]Department of Chemistry, University of Memphis, Memphis, Tennessee

Abstract

Signal transduction modifiers that modulate the lysophosphatidic acid (LPA) pathway have potential as anticancer agents. Herein, we describe metabolically stabilized LPA analogues that reduce cell migration and invasion and cause regression of orthotopic breast tumors *in vivo*. Two diastereoisomeric α-bromophosphonates (BrP-LPA) were synthesized, and the pharmacology was determined for five LPA G protein–coupled receptors (GPCRs). The *syn* and *anti* diastereomers of BrP-LPA are pan-LPA GPCR antagonists and are also nanomolar inhibitors of the lysophospholipase D activity of autotaxin, the dominant biosynthetic source of LPA. Computational models correctly predicted the diastereoselectivity of antagonism for three GPCR isoforms. The *anti* isomer of BrP-LPA was more effective than *syn* isomer in reducing migration of MDA-MB-231 cells, and the *anti* isomer was superior in reducing invasion of these cells. Finally, orthotopic breast cancer xenografts were established in nude mice by injection of MB-231 cells in an *in situ* cross-linkable extracellular matrix. After 2 weeks, mice were treated with the BrP-LPA alone (10 mg/kg), Taxol alone (10 mg/kg), or Taxol followed by BrP-LPA. All treatments significantly reduced tumor burden, and BrP-LPA was superior to Taxol in reducing blood vessel density in tumors. Moreover, both the *anti*- and *syn*-BrP-LPA significantly reduced tumors at 3 mg/kg. [Cancer Res 2009;69(13):5441–9]

Introduction

Lipid signaling in cancer is dominated by the signal transduction through two pathways involving overproduction of two phosphorylated lipids: phosphatidylinositol 3,4,5-trisphosphate (PIP_3) and lysophosphatidic acid (LPA). In both pathways, down-regulated tumor suppressors and up-regulated oncogenes result in a systemic or local overproduction of these potent agonists, and these defects are present in many advanced cancers. Quite recently, therapeutically important inhibitors of the phosphatidylinositol 3-kinase (1) responsible for PIP_3 production have entered the clinic (2). However, anticancer agents that modify signaling through the LPA signaling pathway (3–6) remain in preclinical research, although the molecular understanding of pathway has greatly increased (7).

LPA signaling occurs via six receptors belonging to the seven transmembrane G protein–coupled receptor (GPCR) protein family, now LPA_1 to LPA_6. The first three, LPA_1 to LPA_3, formerly EDG2, EDG4, and EDG7 (8), are expressed from endothelial differentiation genes (*edg*). The recently deorphaned receptors GPR23/P2Y9 (9), GPR92 (10), and GPR87 (11), designated as LPA_4, LPA_5, and LPA_6, belong to the purinergic cluster of GPCRs. Cancer cells of different cellular origins express LPA GPCRs in differing amounts, e.g., LPA_1 is widely expressed in cancer cells, whereas LPA_4 is expressed at low levels. Ovarian and breast cancer cells express multiple LPA GPCR isoforms, and LPA accumulates in tumor cell ascites and effusates (4, 5).

LPA elicits growth factor–like effects in most cell types. LPA is implicated in physiologic responses that include immunologic competence, brain development, wound healing, coagulation, and regulation of blood pressure. The pleiotropic physiologic functions of LPA contribute to pathophysiologic states that include cancer, atherosclerosis, hypertension, ischemia reperfusion injury, and prevention of radiation-induced toxicity (12). As GPCRs, LPA receptors should be amenable to the development of highly specific and potent agonists or antagonists. Validated compounds are essential to advance *in vivo* studies and to minimize off-target effects. To address this need, we developed bioactive analogues of LPA that resist phosphatase, acyl transferase, and lipase activities (13, 14).

LPA and its structural analogues all have a polar head group, a linker, and a hydrophobic tail (Fig. 1*A*). Hydrolysis of the phosphate head group of LPA by ubiquitous phosphatases deactivates LPA, but modifications at this site are the least well tolerated. Stable phosphomimetics that are micromolar or submicromolar LPA agonists include phosphonates, e.g., α-hydroxymethylene phosphonates (15) and α-fluoromethylene phosphonates (16).

Targeting the biosynthesis of LPA is also a valid target for therapeutic development. The lysophospholipase D (lysoPLD) activity of the tumor-associated protein autotaxin (ATX) converts lysophosphatidylcholine (LPC) to LPA (17, 18). ATX is the product of 1 of the 40 most up-regulated genes in invasive cancers and is implicated in cell motility and tumor invasion, metastasis, and neovascularization (19, 20). ATX is feedback inhibited by its product LPA (21). Thus, the ideal anticancer drug targeting LPA signaling would simultaneously abrogate signaling through the GPCRs and attenuate LPA production by ATX (5). Indeed, we previously observed that the palmitoyl α-bromomethylenephosphonate **1** (Fig. 1*A*; BrP-LPA) was a pan-antagonist for LPA_1, LPA_2, LPA_3, and LPA_4 GPCRs (15). This

Note: Supplementary data for this article are available at Cancer Research Online (http://cancerres.aacrjournals.org/).

Requests for reprints: Glenn D. Prestwich, University of Utah, 419 Wakara Way, Suite 205, Salt Lake City, UT 84108. Phone: 801-585-9051; Fax: 801-585-9053; E-mail: gprestwich@pharm.utah.edu.

doi:10.1158/0008-5472.CAN-09-0302

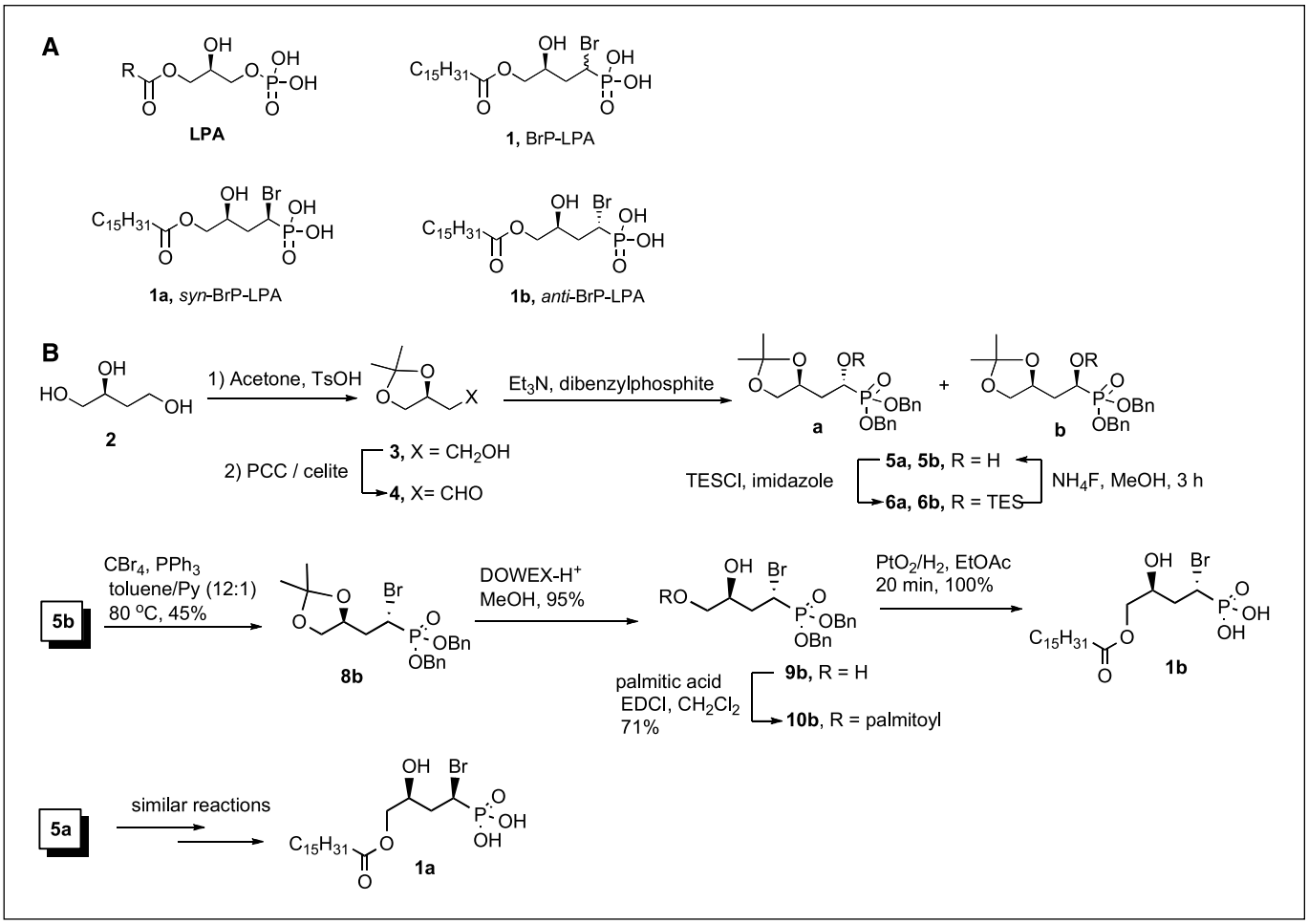

Figure 1. *A,* structures of LPA and stabilized analogues. *B,* synthesis of *syn*- and *anti*-BrP-LPA isomers **1a** and **1b**. See text for experimental details.

diastereomeric mixture also inhibited over 98% of ATX activity at 10 μmol/L.

Herein, we describe the enantioselective syntheses of the *syn* and *anti* diastereomers of BrP-LPA. Computational modeling of the *syn* and *anti* diastereomers predict the independently determined *in vitro* pharmacology and cell biology of these diastereomers. Next, we show that each diastereoisomer inhibits ATX and inhibit cell migration and invasion. Finally, treatment with BrP-LPA diastereomers causes tumor regression and decreased tumor vascularity *in vivo* in an orthotopic breast cancer xenograft model (22, 23).

Materials and Methods

Chemical synthesis. Full experimental details can be found in the Supplementary Data. The final products are described below and summarized in Fig. 1*B*.

(*a*) 1(*S*)-Bromo-3(*S*)-hydroxy-4-(palmitoyloxy)butyl]phosphonate (**1b**). To a solution of phosphonate **10b** (120 mg, 0.18 mmol) in 8 mL EtOAc was added PtO_2 (6 mg). The mixture was stirred under 1 atm H_2 atmosphere for 20 min, filtered, and concentrated to give *anti* isomer **1b** (87 mg, 100%). $[\alpha]_{20}^{D} = -32.1$ (*c* 0.5, $CHCl_3$); ^{1}H NMR (400 MHz, $CDCl_3$) δ 4.11-4.00 (m, 4H), 2.28 (t, *J* = 7.6 Hz, 2H), 2.15-2.08 (m, 1H), 1.94-1.85 (m, 1H), 1.63-1.56 (m, 2H), 1.18 (m, 24H), 0.80 (t, *J* = 7.2 Hz, 3H); ^{13}C NMR (101 MHz, $CDCl_3$) δ 174.6, 68.1, 66.8, 66.7, 40.9, 39.3, 36.6, 34.2, 32.1, 29.8, 29.78, 29.7, 29.6, 29.5, 29.4, 29.3, 25.0, 22.8, 14.1; ^{31}P NMR (162 MHz, $CDCl_3$) δ 20.21 (1P); MALDI-HRMS $[M + Na]^+$ calcd for $C_{20}H_{40}BrO_6PNa$ 509.1638, 511.1621, found 509.1634, 511.1557.

(*b*) 1(*R*)-Bromo-3(*S*)-hydroxy-4-(palmitoyloxy)butyl]phosphonate (**1a**) was obtained from **10a** in 94% yield analogously, as described for compound **1b**. $[\alpha]_{20}^{D} = +3.2$ (*c* 0.5, $CHCl_3$); ^{1}H NMR(400 MHz, $CDCl_3$) δ 4.13 (m, 1H), 4.05-4.00 (m, 2H), 3.95-3.98 (m, 1H), 2.28 (t, *J* = 7.6 Hz, 2H), 2.25-2.08 (m, 2H), 1.54 (m, 2H), 1.18 (m, 24H), 0.80 (t, *J* = 6.8 Hz, 3H); ^{13}C NMR (101 MHz, $CDCl_3$) δ 174.6, 67.6, 67.5, 67.1, 39.5, 37.9, 37.4, 34.2, 32.1, 29.8, 29.78, 29.7, 29.6, 29.5, 29.4, 29.3, 24.98, 22.8, 14.1; ^{31}P NMR (162 MHz, $CDCl_3$) δ 19.64 (1P); MALDI-HRMS $[M + Na]^+$ calcd for $C_{20}H_{40}BrO_6PNa$ 509.1638, 511.1621, found 509.1639, 511.1605.

Receptor activation. Assays for mobilization of intracellular Ca^{2+} were performed as described (15, 24), with details in the Supplementary Data. Each test was performed in quadruplicate. EC_{50}, IC_{50}, and K_i values were calculated by fitting a sigmoid function to data points (25).

Molecular modeling. Docking simulations were performed using Autodock 3.0 (26). The compounds were constructed using MOE with a −2 charge on the phosphate, and geometry was optimized with MMFF94 (27). Each compound was flexibly docked in inactive models (28) of $LPA_{1\text{-}3}$. A mol2 format file of the receptor consisting of the structure coordinates with MMFF94 charges was generated in MOE. The receptor input file was prepared using the molto2pdbqs utility, and ligands were prepared with Autotors. A docking box was defined to encompass the binding site (28). Default parameters of Autodock 3.0 were used, except for energy evaluations (9×10^{10}), genetic algorithm search generations (3×10^4), maximum local search iterations (3×10^3), and 15 runs. A single complex was selected for each ligand-receptor combination based on both rank and proximity of ligand phosphate group to R3.28. Usually, the top-ranked structure showed close interaction with R3.28 and was selected. For

1a-LPA_3, the second-ranked structure was selected. The selected complexes were minimized with MMFF94 and interactions were analyzed.

ATX assay. Using FS-3 (ref. 29; Echelon Biosciences, Inc.) as substrate and recombinant hemagglutinin-tagged ATX (ATX-HA), 50 μL of ATX-HA (0.25 μg) in assay buffer [Tris 50 mmol/L, NaCl 140 mmol/L, KCl 5 mmol/L, $CaCl_2$ 1 mmol/L, $MgCl_2$ 1 mmol/L (pH 8.0)] was mixed with 25 μL of FS-3 (final, 1 μmol/L) and 25 μL of test compound dissolved in assay buffer with 1:1.5 bovine serum albumin in 96-well plate. FS-3 fluorescence at excitation and emission wavelengths of 485 and 538 nm, respectively, were monitored using a FLEXstation II for 2 h of incubation at 37°C. The differences between time of 0 and 120 min were calculated individually and normalized to the vehicle control. The mean ± SD of triplicate sample wells was expressed as percentage of ATX inhibition. Significant difference compared with vehicle was determined by the Student's *t* test at a *P* value of 0.05 (25).

Scratch wound assay. MDA-MB-231 cells were plated in triplicate into six-well plates at 3×10^5 per well. At 48 h, the confluent cell layer was scratched using a sterile pipette tip. Nonadherent cells and cellular debris were removed by washing (PBS). Fresh medium containing BrP-LPA **1**, *syn*-BrP-LPA **1a**, or *anti*-BrP-LPA **1b** (1–100 μmol/L) was added to the scratched monolayers. Cells were observed and digitally photographed. Inhibition of migration was assessed and quantified by using ImageJ (30).

Xenograft establishment and chemotherapy. Female *nu/nu* mice (ages, 4–6 wk; Charles River Laboratories) were anesthetized by i.p. injection of ketamine (80 mg/kg) and xylazine (10 mg/kg), as approved by the University of Utah Institutional Animal Care and Use Committee. Before inoculation, MDA-MB-231 cells were trypsinized and resuspended in Extracel (Glycosan BioSystems) with a final concentration of 5×10^7 cells/mL, and the resulting suspension was mixed gently. An aliquot of 200 μL of the mixture was injected s.c. into the fourth mammary fat pad of each mouse. The mice were randomly divided into treatment groups and control groups (six mice per group). Treatments were Taxol (10 mg/kg), BrP-LPA **1** (10 mg/kg), or Taxol (10 mg/kg) followed by BrP-LPA **1** (10 mg/kg). The control was physiologic saline. Injections (i.p.) were performed twice per week for 2 wk, starting 2 wk after the cell transplantation. Tumor sizes were measured and calculated: tumor size (mm^3) = [width (mm)]^2 × [length (mm)] / 2. After sacrifice, tumor tissue was removed for histogical H&E and immunohistochemistry using an anti-CD31 antibody. CD31 in zinc-fixed paraffin sections was detected using antirat immunoglobulin horseradish peroxidase detection kit (BD Bioscience). Microvessels were counted at ×400 magnification, and the data were converted to microvessel density (vessels/mm^2), with 1 microscopic field = 0.196 mm^2. Six fields were randomly chosen for quantification in three slides for each treatment group tumor tissue.

The effect of *syn*-BrP-LPA **1a** and *anti*-BrP-LPA **1b** were evaluated separately after an analogous protocol. The cell suspension injection volume was reduced to 100 μL, and dosages were 3 mg/kg for **1a** and **1b**.

Statistical methods. Data from *in vitro* and *in vivo* experiments are expressed as the mean ± SD of at least triplicate determinations. Statistical comparisons were performed by Student's *t* test, and differences were considered significant at $P < 0.05$.

Results

Diastereoselective synthesis and absolute stereochemistry. The synthesis of the individual diastereoisomers **1a** (*syn*) and **1b** (*anti*) used a stereocontrolled bromination of the separated α-hydroxymethylene phosphonates (Fig. 1*B*). Aldehyde **4** was prepared in two steps in high yield from acetonide **3** and converted to the diastereomeric mixture of α-hydroxymethylene phosphonates **5a** and **5b**. Although this mixture was not readily separable, the TES ethers **6a** and **6b** could be separated by flash chromatography, and the silyl group could be readily removed. Using purified isomer **5b**, bromination was performed at high dilution (1 g of **5b** in 80 mL) in 12:1 toluene:pyridine to optimize the yield (Fig. 1*B*). After acetonide deprotection, selective palmitoylation, and hydrogenation, the pure *anti* diastereomer **1b** was obtained in quantitative yield. The *syn* diastereoisomer **1a** was obtained similarly, starting with **5a**.

The stereochemical assignment of the absolute configuration of α-position was accomplished by two-dimensional NMR analysis of 1,3-diol acetonide (31, 32). Thus, isomer **6b** was converted in several steps (deprotection, selective silylation, acetonide formation) to acetonide **7b** (Supplementary Fig. S1). The absolute configuration of the α-C in **7b** was confirmed by coupling constants and ^1H-^1H NOESY. Specifically, NOEs were observed between H_1 and H_3, H_1 and H_{2e}, and H_3 and H_{2e}, establishing a *syn*-1,3-relationship in phosphonate **7b**. In **7a**, no NOEs were observed between H_1 and H_3, confirming the *anti*-1,3 relative stereochemistry. In addition, the acetonide methyls of **7b** displayed ^{13}C NMR chemical shifts characteristic of the acetonide of a *syn*-1,3-diol (31).

Receptor activation assays. The ligand properties of the compounds were evaluated using a Ca^{2+} mobilization assay to assess activation or inhibition of LPA_1, LPA_2, LPA_3, and LPA_5 expressed in RH7777 cells and LPA_4 expressed in Chinese hamster ovary (CHO) cells. Table 1 illustrates calcium responses elicited through the response of human LPA_1, LPA_2, LPA_3, LPA_4, and LPA_5 receptors to *syn*-BrP-LPA **1a**, *anti*-BrP-LPA **1b,** and BrP-LPA **1**. These cell lines are used extensively for characterization of LPA GPCR ligands, because RH7777 cells are intrinsically unresponsive

Table 1. Pharmacological results with **1**, **1a**, and **1b**

	LPA_1	LPA_2	LPA_3	LPA_4	LPA_5	ATX
1	Antagonist IC_{50}: 4520 ± 1521 nmol/L K_i: 805 nmol/L	Antagonist IC_{50}: 468 ± 322 nmol/L K_i: 245 nmol/L	Antagonist 71.3% inhibition at 30 μmol/L (200 nmol/L LPA)	Antagonist 13.9% inhibition at 30 μmol/L (400 nmol/L LPA)	Partial agonist EC_{50}: 1282 ± 222 nmol/L E_{max}: 54% at 10 μmol/L	102 ± 2.7% inhibition (10 μmol/L)
1a	Antagonist IC_{50}: 648 ± 475 nmol/L K_i: 273 nmol/L	Antagonist IC_{50}: 288 ± 103 nmol/L K_i: 250 nmol/L	Antagonist IC_{50}: 4440 ± 1850 nmol/L K_i: 1830 nmol/L	Antagonist 35.1% Inhibition at 30 μmol/L (400 nmol/L LPA)	Partial agonist NS E_{max}: 64% at 10 μmol/L	98.1 ± 2.3% inhibition (10 μmol/L)
1b	Antagonist IC_{50}: 2079 ± 1544 nmol/L K_i: 752 nmol/L	Antagonist IC_{50}: 275 ± 133 nmol/L K_i: 241 nmol/L	Antagonist IC_{50}: 2089 ± 1212 nmol/L K_i: 623 nmol/L	Antagonist 33.1% Inhibition at 30 μmol/L (400 nmol/L LPA)	Antagonist IC_{50}: 977 ± 493 nmol/L K_i: 376 nmol/L	99.4 ± 2.7 % Inhibition (10 μmol/L)

Abbreviation: NS, non-saturated.

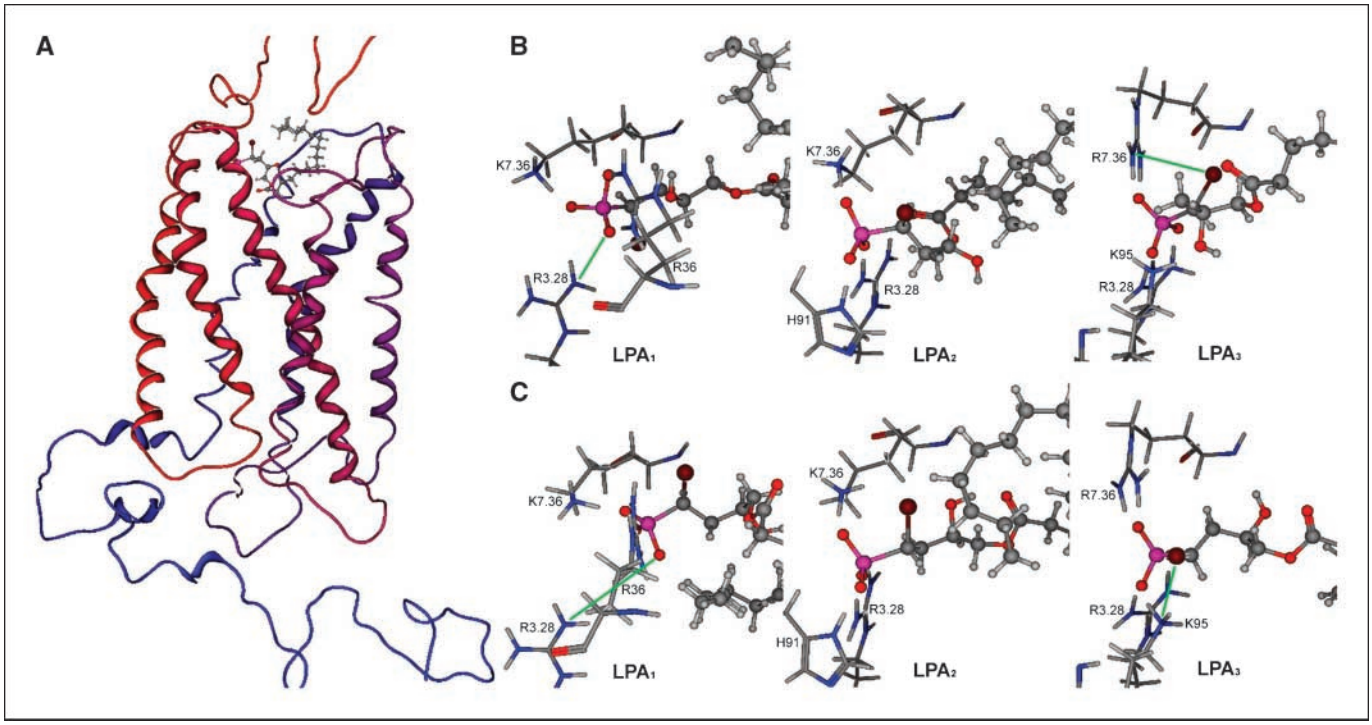

Figure 2. Docked complexes of *syn*-**1a** and *anti*-**1b** in LPA_{1-3} accurately predict pharmacology. *Syn*-**1a** and *anti*-**1b** are ball-and-stick models, receptor residues are labeled stick models, and ribbons show the protein backbone (*red,* amino terminus; *blue,* carboxy terminus). *A,* typical view shows the *syn* isomer **1a** in the LPA_2 receptor, with the ligand positioned at the interface between the transmembrane α-helical segments and the extracellular loops (*top*). *B* and *C,* close views of *syn*-**1a** and anti-**1b**, respectively, docked in the LPA_{1-3} receptors as viewed from the extracellular side. Interactions differing significantly between the complex of each receptor with **1a** and **1b** have green lines.

to LPA, whereas wild-type CHO cells show minimal endogenous responses to LPA (5, 9, 25, 33).

The diastereomeric mixture BrP-LPA **1** (prepared from unseparated isomers **5a** and **5b**) showed pan-antagonist activity for stably transfected receptors LPA_{1-4} submicromolar potency toward LPA_2, modest inhibition of LPA activation of LPA_4, and weak partial agonism for the transiently transfected LPA_5. The *syn*-BrLPA **1a** was a pan-antagonist for the *edg* family GPCRs, showing K_i values of 273, 250, and 1830 nmol/L for LPA_1, LPA_2, and LPA_3, respectively. For the purinergic family GPCRs, *syn*-BrLPA **1a** was an antagonist for LPA_4 but a weak agonist for LPA_5. Apparently, the overall agonist effect dominates in the mixed diastereomers. By comparison, *anti*-BrP-LPA **1b** was a pan-antagonist for the *edg* family GPCRs, with K_i values of 752, 241, and 623 nmol/L for LPA_1, LPA_2, and LPA_3, respectively. In addition, *anti*-BrP-LPA **1b** was an antagonist for the two purinergic family GPCRs, with partial antagonism of LPA on LPA_4 and a K_i value of 376 nmol/L for LPA_5.

Molecular modeling of diastereoisomers with LPA_1, LPA_2, and LPA_3. Molecular models of the complexes formed by *syn*-BrP-LPA **1a** and *anti*-BrP-LPA **1b** with LPA_{1-3} were created without prior knowledge of the pharmacologic results. The models showed ionic interactions between the **1a** or **1b** phosphate groups and basic residues in the NH_2 terminus, third transmembrane domain, and seventh transmembrane domain in LPA_{1-3} (Fig. 2). The basic NH_2 terminal residues showed variable position and type, with LPA_1 interacting via R36, LPA_2 interacting via H91, and LPA_3 interacting via K95. The interacting residue in the third transmembrane domain is the conserved arginine appearing at position 3.28, a residue that is critical for both LPA recognition by EDG family LPA receptors (34–36) and S1P recognition by the EDG family S1P receptors (36, 37). The interacting residue in the seventh transmembrane domain of LPA_1 and LPA_2 is K7.36, whereas LPA_3 uses R7.36. Moreover, K7.35 in LPA_3, not R7.36, is essential for LPA recognition, although this lysine is replaced by an acidic residue in LPA_1 and LPA_2 (36). The hydrophobic tails interact primarily with residues in the extracellular loops, consistent with previous models of LPA receptor antagonism (24, 25, 28). The geometries of these complexes accurately predicted that both *syn*-BrP-LPA **1a** and *anti*-BrP-LPA **1b** would antagonize LPA action at all three EDG family LPA receptors by competing for interaction at R3.28 and without independent agonist activity due to their lack of hydrophobic interactions within the transmembrane domain.

Inhibition of ATX. The inhibition of ATX by BrP-LPA **1**, *syn*-BrP-LPA **1a**, and *anti*-BrP-LPA **1b** was measured at concentrations of 0.01 to 10 μmol/L and compared with the ATX inhibitory effects of 10 μmol/L LPA (18:1) and 10 μmol/L 2ccLPA (16:1; ref. 38; Supplementary Fig. S2). ATX activity was measured by the hydrolysis of the fluorogenic lysoPC analogue **FS-3**, with a K_m value of 6.3 μmol/L (29). Preliminary results showed that each analogue inhibited >98% of ATX at 10 μmol/L. A clear dose-response effect on inhibition was observed for both *syn*-BrP-LPA **1a** (IC_{50} = 165 nmol/L) and *anti*-BrP-LPA **1b** (IC_{50} = 22 nmol/L; Supplementary Fig. S2).

Inhibition of migration. BrP-LPA can both significantly reduce LPA production and block activation of cell surface LPA receptors. Such a molecule has clear therapeutic potential to reduce LPA-induced cell migration, invasion, and proliferation (5, 38, 39). Thus, we evaluated the effect of the analogues on MDA-MB-231 breast cancer cells using a scratch wound assay (Fig. 3*A*). The relative expression of LPA GPCRs in MDA-MB-231 cells is LPA_1 > LPA_2 >>

LPA_3, and LPA_1 seems to be the key in mediating cell migration of normal and neoplastic cells (40). After treatment with pure diastereomers **1a** and **1b** and the mixture BrP-LPA **1**, cells were allowed to migrate into the denuded area for 0, 16, and 24 hours. By 24 hours, untreated control cells completely filled the scratched area. Treatment with *syn*-BrP-LPA **1a** and *anti*-BrP-LPA **1b** at 10 and 40 μmol/L inhibited the MDA-MB-231 cell migration (Fig. 3*B*). Migration of MB-231 cells was decreased by 57% ($P < 0.05$) by 40 μmol/L *anti*-BrP-LPA **1b** when compared with the untreated control. The mixed diastereomers showed intermediate inhibition of cell migration (data not shown).

Inhibition of invasion. Using an *in vitro* invasion assay, MDA-MB-231 cells invaded through Matrigel-coated transwell membranes (Supplementary Fig. S3). Treatment with *anti*-BrP-LPA **1a** or *syn*-BrP-LPA **1b** inhibited the invasion by ~52% ($P < 0.05$), but the potencies of the two isomers were not significantly different. This suggests that connecting the complex biology of invasion to specific aspects of pharmacology of individual receptors or ATX inhibition will require additional investigation.

Tumor regression in engineered orthotopic breast tumor xenografts. To evaluate BrP-LPA *in vivo*, we used "tumor engineering" to create orthotopic breast tumors in nude mice (22, 23). In the first experiment, we compared BrP-LPA **1** alone with Taxol alone. We also simulated a dual-drug therapy approach by administering Taxol followed by the mixed diastereomers **1**. Thus, s.c. mammary fat pad injection of MDA-MB-231 cells suspended in a semisynthetic extracellular matrix (sECM, Extracel) in *nu/nu* mice resulted in tumor growth at each injection site. Figure 4 shows the increase in tumor volumes during the growth phase and decrease in tumor volumes during the treatment phase. During the first 2 wk, the tumor cells expand within the volume of the injected sECM. The gross size of the bolus changes little, but the tumor cell density increases dramatically as cells proliferate, degrade the sECM, and secrete their own ECM. After 2 weeks of tumor growth, the control group was treated with four i.p. injections of physiologic saline over the course of 2 weeks. The first treatment group received i.p. injections of Taxol (10 mg/kg), and the second treatment group received i.p. injections of BrP-LPA **1** (10 mg/kg), twice per week for 2 weeks. The third treatment group received two injections of Taxol (10 mg/kg) for week 1 and two injections of BrP-LPA **1** (10 mg/kg) for week 2. In each of the three treatment groups, a reduction of tumor size relative to controls was observed shortly after the first therapeutic injection (Fig. 4*A*).

To examine the separate effects of the two diastereomers, *syn*-BrP-LPA **1a** and *anti*-BrP-LPA **1b**, a second xenograft study was performed using analogous protocols, except that the size of the

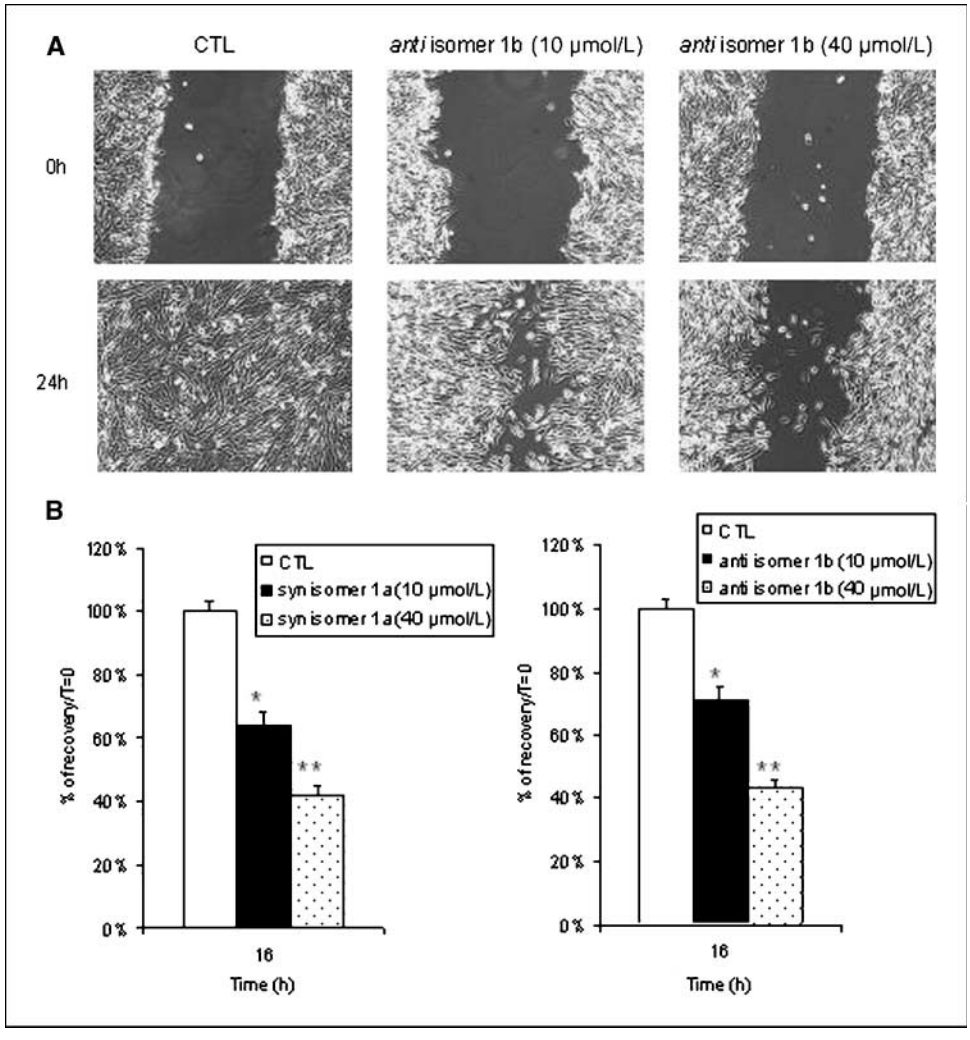

Figure 3. Effect of *syn*-**1a** and *anti*-**1b** BrP-LPA diastereomers on MDA-MB-231 cell migration. *A,* confluent MDA-MB-231 cells were scratched and then treated with *syn*-**1a** or *anti*-**1b** (10 and 40 μmol/L) and compared with untreated cells (*CTL*) at 24 h. *B,* quantification for the *anti*-BrP-LPA **1b** and *syn*-BrP-LPA **1a**. Asterisks indicate significant differences from control (*CTL*) at $P < 0.0005$ (*) and $P < 0.0001$ (**) for *syn* isomer **1a** and at $P < 0.001$ (*) and $P < 0.0001$ (**) for *anti*-isomer **1b**.

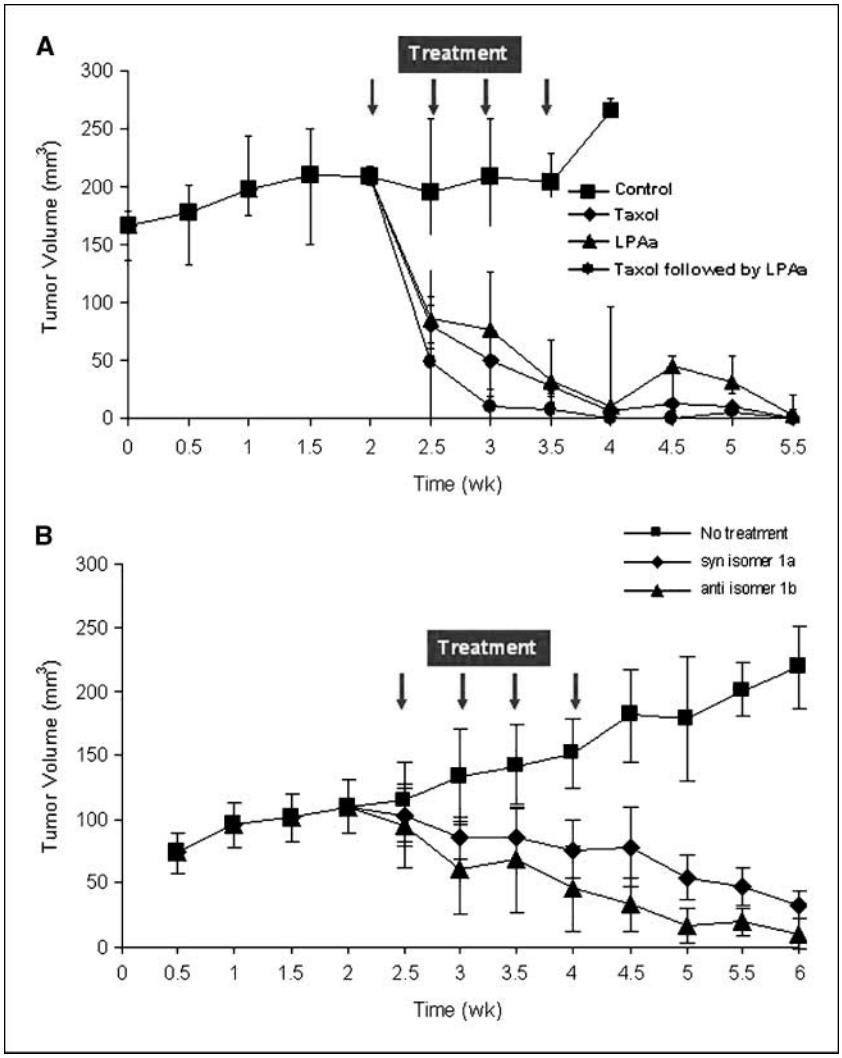

Figure 4. BrP-LPA treatment reduces tumor size in orthotopic breast cancer xenografts. *A,* effect of BrP-LPA **1** treatment (10 mg/kg i.p.) on MDA-MB-231 tumor growth *in vivo*. At 6 wk, all tumor volumes in treated animals were significantly different from the controls but not different from each other ($P < 0.05$). *B,* effect of *syn*-BrP-LPA **1a** and *anti*-BrP-LPA **1b** treatment (3 mg/kg i.p.) on MDA-MB-231 tumor growth. At 6 wk, **1a** and **1b** were statistically different from controls ($P < 0.05$) but not from each other ($P = 0.16$).

injected cell suspension was reduced to 100 μL and the treatment dosage was reduced to 3 mg/kg. Figure 4*B* shows that, although each isomer significantly decreased the tumor volume relative to the control group ($P < 0.01$), there was no significant difference between the tumor reduction by **1b** relative to **1a** for this experimental group size ($P = 0.16$). As observed in the invasion assay, the *in vivo* biology can often be more complex that the sum of individual receptor pharmacology and enzyme inhibition outcomes.

After completion of the 2-week treatment course for the study in Fig. 4*A* comparing the Taxol and BrP-LPA treatments, tumors in each treatment group were significantly decreased or undetectable. At necropsy, tumors were surgically removed and prepared for histologic analysis. The largest tumor in the treatment group with diastereomeric mixture **1** was significantly smaller than the smallest tumor in the control group (Fig. 5*A*). H&E staining revealed an irregular arrangement of tumor cells, inflammatory granuloma tissue, and an increased number of blood vessels (Fig. 5*B*) in the control group. An endothelial layer covering tumor vasculature was observed using immunohistochemical staining with anti-CD31 antibody (Fig. 5*C*). Quantification of the newly generated vessels in the tumor samples in six different fields of three slides for each treatment group (Fig. 5*D*) showed highly significant reduction of angiogenesis in the mice treated with the LPA antagonist mixture **1** relative to the controls or either of the Taxol treatments ($P < 0.01$).

Discussion

Computational modeling predicts pharmacology. The docking of *syn*-BrP-LPA **1a** and BrP-LPA **1b** with GPCRs $LPA_{1\text{-}3}$ were performed computationally without knowledge of the pharmacologic outcomes. The predictions from the models were gratifyingly congruent with the relative antagonist activity at $LPA_{1\text{-}3}$, lending credibility to the predictive power of the model. Distances between phosphate groups of **1a** and **1b** and basic residues in each LPA receptor model provide a molecular context for the relative potencies observed experimentally (Fig. 2; Supplementary Table 1). For example, the phosphate of **1a** interacts more closely with the cationic residue in transmembrane domain 3, consistent with greater antagonism. The interaction distances for **1a** and **1b** with LPA_2 are essentially identical, consistent with equivalent potencies. Whereas both compounds show similar phosphate basic residue distances in LPA_3, the partially negative bromine atom of **1b** is only 2.5 Å from K95. In contrast, the bromine atoms in the other five complexes are >3.5 Å from the basic residues, consistent with the more potent antagonism of **1b** compared with **1a**.

Unique LPA antagonists. To our knowledge, this constitutes the first comprehensive pharmacologic assessment of novel analogues of LPA on five LPA GPCRs from two families. Notably, diastereomer **1b** is the first known pan-antagonist, blocking LPA activation at $LPA_{1\text{-}5}$. This represents a proof of concept that compounds capable of inhibiting both the *edg* family of LPA receptors ($LPA_{1\text{-}3}$) and the purinergic family of LPA receptors represented by LPA_4 and LPA_5 exist.

BrP-LPA diastereomers differentially inhibit ATX and cell migration. LPA is produced from LPC by ATX/lysoPLD (17, 18, 41), and local production of LPA can support invasion of tumor cells, promoting metastasis (4, 19, 42) via several molecular mechanisms. First, activation of the Rho and Rac GTPase pathways downstream from LPA-GPCRs regulates actin cytoskeleton and cell motility (43). Second, LPA modulates the activity of matrix metalloproteinases, which are crucial for metastasis and LPA-induced transphosphorylation of the epidermal growth factor receptor (44). Third, the potent motogenic effects of ATX are lead to enhanced angiogenesis (45). Thus, LPA receptor antagonists and ATX inhibitors have potential in cancer therapy both by blocking the growth-supporting, angiogenic, and antiapoptotic effects of LPA and by reducing its titer (42, 46).

Addition of BrP-LPA diastereomers **1a** and **1b** at 40 μmol/L both significantly decreased migration of MDA-MB-231 cells into a scratched monolayer. The more potent ATX inhibitor *anti*-BrP-LPA **1b** showed greater potency in reducing cell migration, although the isomers were equipotent in decreasing the cell invasion through Matrigel-coated transwell membranes.

BrP-LPA diastereomers cause tumor regression and reduced angiogenesis. Finally, the BrP-LPA diastereomers were evaluated in a xenograft model using engineered orthotopic breast tumors in nude mice (22, 23). This new model has potential for creating vascularized, orthotopic tumors from patient-derived samples and offers a method to introduce labeled metastatic cells into any organ (47). We first used the mixed diastereomers **1** to compare buffer injection with 10 mg/kg i.p. doses, BrP-LPA alone (four doses), Taxol alone (four doses), and Taxol (two doses) followed by BrP-LPA (two doses). The tumors in all treatment groups were significantly decreased. Interestingly, quantification of the newly generated blood vessels in the tumor samples showed highly significant reduction of angiogenesis in the mice treated with BrP-LPA **1** relative to either the controls or Taxol treatments ($P < 0.01$). To rationalize this observation that the Taxol followed by BrP-LPA has the same effect as Taxol alone, we note that Taxol is a mitotic poison, whereas BrP-LPA inhibits signaling pathways important for proliferation, migration, and angiogenesis; this compound likely requires actively dividing cells to exert its effect. Apparently, in tumors with cells in a growth arrested/apoptotic state, no additional effect of the BrP-LPA was possible.

This result is extremely encouraging in view of the requirement for ATX in blood vessel formation during embryogenesis (48) and the growing potential of antiangiogenic drugs, e.g., Avastin, in cancer therapy. In addition, each diastereomer significantly decreased the tumor volume relative to the control group ($P < 0.01$) at 3 mg/kg. However, with six mice per group, only a trend was evident to suggest that *anti*-BrP-LPA **1b** might be more

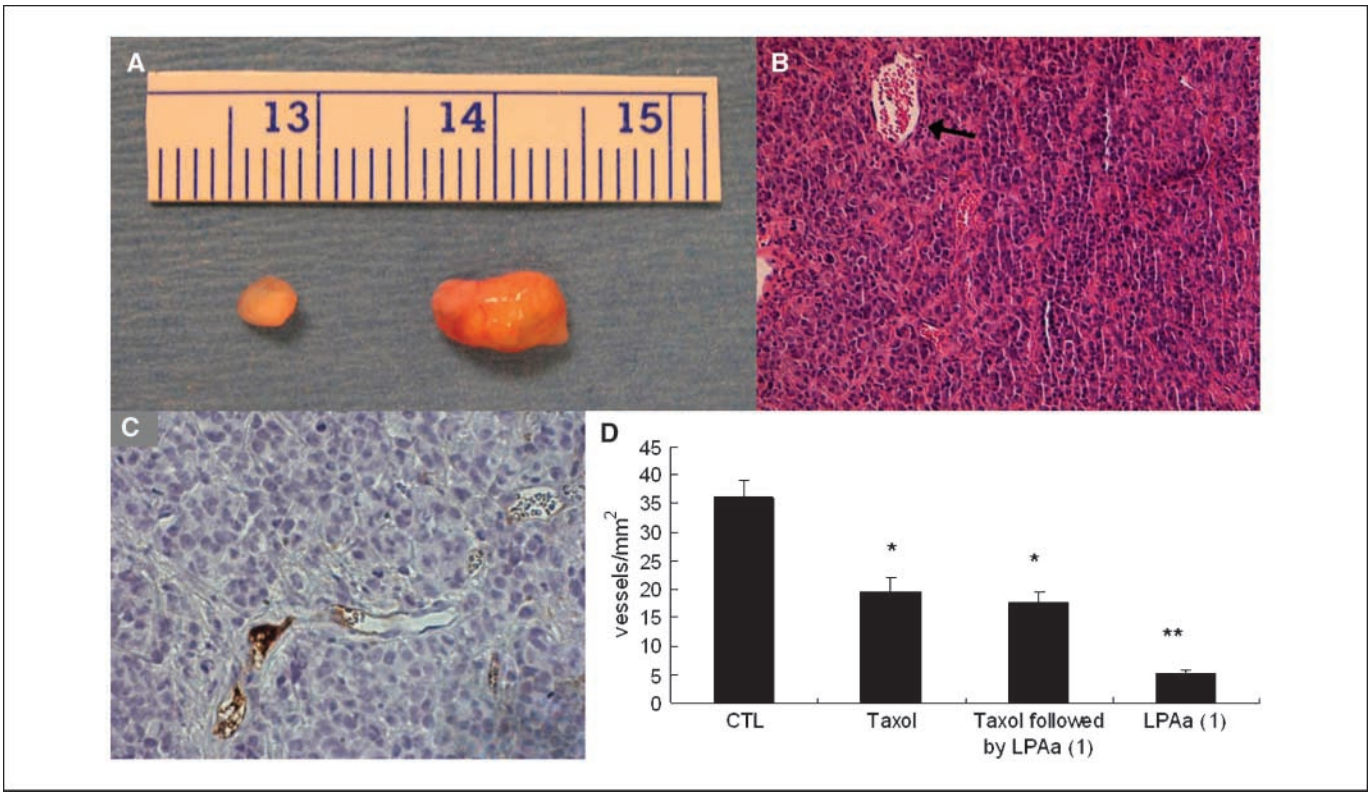

Figure 5. BrP-LPA decreases tumor size and vascularity. *A,* difference in gross tumor size. H&E staining (*B*) and CD31-specific staining (*C*) show relative angiogenesis. *D,* quantification of newly generated vessels in the tumor samples. The asterisk (*) indicates that Taxol alone and Taxol then BrP-LPA **1** (mixed isomers) were statistically different from the control ($P < 0.05$) but not different from each other. Treatment with BrP-LPA **1** alone showed significantly lower blood vessel density (**) than the controls ($P < 0.001$) or either Taxol treatment ($P < 0.05$).

higher efficacy relative to *syn*-BrP-LPA **1a** ($P < 0.1$). The mechanistic basis for the antiangiogenic effects of the BrP-LPA isomers are the subject of active studies with other tumor cells and other matrices.

Therapeutic potential of ATX inhibitors and LPA antagonists in cancer treatment. LPA GPCRs and ATX present two promising, druggable, yet underexploited targets for cancer therapy (5, 6). ATX, a potent motogen in metastatic cancers (19) produces a continuous output of LPA (17, 18), potentially abrogating the action of an LPA antagonist. By blocking ATX, the autocrine/paracrine loop that involves the ATX-mediated production of LPA is reduced (42, 46). Although ATX is product feedback inhibited (21), using LPA to inhibit ATX would be counterproductive. Thus, analogues of LPA that retained ATX inhibitory activity, yet did not activate LPA GPCRs, are needed. Recently, a structure-function study of carbacyclic analogues of cyclophosphatidic acid (ccPA) showed that these compounds were selective inhibitors of ATX and lacked agonist activity for $LPA_{1,2,3}$ (38). Importantly, ccPA inhibited cancer cell invasion *in vitro* and suppressed metastasis of melanoma cells *in vivo*. However, ATX inhibition alone was inadequate to accomplish both dampen LPA production and suppress receptor activation by endogenous LPA. In a separate study, different small-molecule ATX inhibitors were found to reduce melanoma cell migration *in vitro* (39).

In conclusion, we established that stereoisomers of BrP-LPA, in particular *anti*-BrP-LPA **1b**, simultaneously inhibited ATX and antagonized five of the known LPA GPCRs *in vitro*. Moreover, we established *in vivo* efficacy of the targeted polypharmacology (49) concept for the LPA pathway by showing the regression and reduction of angiogenesis in tumor xenografts. Taken together, these data provide the first proof of concept for the use of a dual-function pan-LPA receptor antagonist and ATX inhibitor in cancer chemotherapy.

Disclosure of Potential Conflicts of Interest

G. Tigyi is an equity holder in RxBio. G.D. Prestwich is an equity holder in Glycosan BioSystems and advisor to RxBio and Echelon Biosciences. The other authors declared no potential conflicts of interest.

Acknowledgments

Received 1/25/09; revised 3/30/09; accepted 4/27/09; published OnlineFirst 6/9/09.

NIH grants HL070231 and NS29632 (G.D. Prestwich), CA921160 and HL61469 (G. Tigyi), and HL0084007 (A.L. Parrill).

Note: The costs of publication of this article were defrayed in part by the payment of page charges. This article must therefore be hereby marked *advertisement* in accordance with 18 U.S.C. Section 1734 solely to indicate this fact.

We thank Echelon Biosciences for FS-3, Glycosan BioSystems for Extracel, T. Shimizu (University of Tokyo) for CHO cells expressing LPA_4, R. Bandle (National Cancer Institute) for HA-tagged ATX, D. Baker for advice on ATX assays, and the Chemical Computing Group for the MOE software.

References

1. Drees BE, Mills GB, Rommel C, Prestwich GD. Therapeutic potential of phosphoinositide 3-kinase inhibitors. Expert Opin Ther Patents 2004;14:703–32.
2. Maira S-M, Stauffer F, Brueggen J, et al. Identification and characterization of NVP-BEZ235, a new orally available dual phosphatidyl 3-kinase/mammalian target of rapamycin inhbitor with potent *in vivo* antitumor activity. Mol Cancer Ther 2008;7:1851–63.
3. Feng L, Mills GB, Prestwich GD. Modulators of lysophosphatidic acid signaling. Expert Opin Ther Patents 2003;13:1619–34.
4. Mills GB, Moolenaar WH. The emerging role of lysophosphatidic acid in cancer. Nat Rev Cancer 2003; 3:582–91.
5. Umezu-Goto M, Tanyi J, Lahad J, et al. Lysophosphatidic acid production and action: validated targets in cancer? J Cell Biochem 2004;92:1115–40.
6. Murph M, Tanaka T, Liu S, Mills GB. Of spiders and crabs: the emergence of lyosphospholipids and their metabolic pathways as targets for therapy in cancer. Clin Cancer Res 2006;12:6598–602.
7. Tigyi G, Parrill AL. Molecular mechanisms of lysophosphatidic acid action. Prog Lipid Res 2003;42: 498–526.
8. Contos JJ, Ishii I, Chun J. Lysophosphatidic acid receptors. Mol Pharmacol 2000;58:1188–96.
9. Noguchi K, Ishii S, Shimizu T. Identification of p2y9/GPR23 as a novel G protein-coupled receptor for lysophosphatidic acid, structurally distant from the Edg family. J Biol Chem 2003;278:25600–6.
10. Lee C-W, Rivera R, Gardell S, Dubin A, Chun J. GPR92 as a new G12/13 and Gq coupled lysophosphatidic acid receptor that increases cAMP: LPA5. J Biol Chem 2006; 281:23589–97.
11. Tabata K, Baba K, Shiraishi A, Ito M, Fujita N. The orphan GPCR GPR87 was deorphanized and shown to be a lysophosphatidic acid receptor. Biochem Biophys Res Commun 2007;363:861–6.
12. Mills GB, Eder A, Fang X, et al. Critical role of lysophospholipids in the pathophysiology, diagnosis, and management of ovarian cancer. Cancer Treat Res 2002;107:259–83.
13. Prestwich GD, Xu Y, Qian L, Gajewiak J, Jiang G. New metabolically stabilized analogs of lysophosphatidic acid: agonists, antagonists, and enzyme inhibitors. Biochem Soc Trans 2005;33:1357–61.
14. Prestwich GD, Gajewiak J, Zhang H, Yang G, Serban MA. Phosphatase-resistant analogues of lysophosphatidic acid: agonists promote healing, antagonists and autotaxin inhibitors treat cancer. Biochim Biophys Acta 2008;1781:588–94.
15. Jiang G, Xu Y, Fujiwara Y, et al. α-Substituted phosphonate analogues of lysophosphatidic acid (LPA) selectively inhibit production and action of LPA. Chem Med Chem 2007;2:679–90.
16. Xu Y, Aoki J, Shimizu K, et al. Structure-activity relationships of fluorinated lysophosphatidic acid analogues. J Med Chem 2005;48:3319–27.
17. Tokumura A, Kanaya Y, Miyake M, Yamano S, Irahara M, Fukuzawa K. Increased production of bioactive lysophosphatidic acid by serum lysophospholipase D in human pregnancy. Biol Reprod 2002;67:1386–92.
18. Aoki J, Taira A, Takanezawa Y, et al. Serum lysophosphatidic acid is produced through diverse phospholipase pathways. J Biol Chem 2002;277:48737–44.
19. Nam S, Clair T, Campo C, Lee H, Liotta L, Stracke M. Autotaxin (ATX), a potent tumor motogen, augments invasive and metastatic potential of ras-transformed cells. Oncogene 2000;19:241–7.
20. Tanaka M, Okudaira S, Kishi Y, et al. Autotaxin stabilizes blood vessels and is required for embryonic vasculature by producing lysophosphatidic acid. J Biol Chem 2006;281:25822–30.
21. van Meeteren LA, Ruurs P, Christodoulou E, et al. Inhibition of autotaxin by lysophosphatidic acid and sphingosine 1-phosphate. J Biol Chem 2005;280:21155–61.
22. Liu Y, Shu XZ, Prestwich GD. Tumor engineering: orthotopic cancer models in mice using cell-loaded, injectable, cross-linked hyaluronan derived hydrogels. Tissue Eng 2007;13:1091–101.
23. Prestwich G. Evaluating drug toxicity and efficacy in three dimensions: using synthetic extracellular matrices in drug discovery. Acc Chem Res 2008;41:139–48.
24. Durgam GG, Virag T, Walker MD, et al. Synthesis, structure-activity relationships, and biological evaluation of fatty alcohol phosphates as lysophosphatidic acid receptor ligands, activators of PPARγ and inhibitors of autotaxin. J Med Chem 2005;48:4919–30.
25. Virag T, Elrod DB, Liliom K, et al. Fatty alcohol phosphates are subtype-selective agonists and antagonists of lysophosphatidic acid receptors. Mol Pharmacol 2003;63:1032–42.
26. Morris G, Goodsell D, Halliday R, et al. Automated docking using a Lamarckian genetic algorithm and an empirical binding free engery function. J Comput Chem 1998;19:1639–62.
27. Halgren T. Merck molecular force field. I. Basis, form scope, parameterization, and performance of MMFF94. J Comput Chem 1996;17:490–519.
28. Sardar VM, Bautista DL, Fischer DJ, et al. Molecular basis for lysophosphatidic acid receptor antagonist selectivity. Biochim Biophys Acta 2002;1582:309–17.
29. Ferguson CG, Bigman CS, Richardson RD, van Meeteren L, Moolenaar WH, Prestwich GD. Fluorogenic phospholipid substrate to detect lysophospholipase D/autotaxin activity. Org Lett 2006;8:2023–6.
30. Denker SP, Barber DL. Cell migration requires both ion translocation and cytoskeletal anchoring by the Na-H exchanger NHE1. J Cell Biol 2002;159:1087–96.
31. Rychnovsky SD, Griesgraber G, Schlegel R. Stereochemical determination of roflamycoin: ^{13}C acetonide analysis and synthetic correlation. J Am Chem Soc 1995;117:197–210.
32. Rychnovsky SD, Richardson TI, Rogers BN. Two-dimensional NMR analysis of acetonide derivatives in the stereochemical assignment of polyol chains: the absolute configurations of dermostatins A and B. J Org Chem 1997;62:2925–34.
33. Fischer DJ, Nusser N, Virag T, et al. Short-chain phosphatidates are subtype-selective antagonists of lysophosphatidic acid receptors. Mol Pharmacol 2001; 60:776–84.
34. Durgam GG, Tsukahara R, Makarova N, et al. Synthesis and pharmacological evaluation of second-generation phosphatidic acid derivatives as lysophosphatidic acid receptor ligands. Bioorg Med Chem Lett 2006;16:633–40.
35. Wang D, Lorincz Z, Bautista DL, Liliom K, Tigyi G, Parrill AL. A single amino acid determines ligand specificity of the S1P1 (EDG1) and LPA1 (EDG2) phospholipid growth factor receptors. J Biol Chem 2001;276:49213–20.
36. Fujiwara Y, Sardar V, Tokumura A, et al. Identification of residues responsible for ligand recognition and regioisomeric selectivity of lysophosphatidic acid receptors expressed in mammalian cells. J Biol Chem 2005;280:35038–50.

37. Parrill AL, Wang D-A, Bautista DL, et al. Identification of edg1 receptor residues that recognize sphingosine 1-phosphate. J Biol Chem 2000;275:39379–84.
38. Baker D, Fujiwara Y, Pigg KR, et al. Carba analogs of cyclic phosphatidic acid are selective inhibitors of autotaxin and cancer cell invasion and metastasis. J Biol Chem 2006;281:22786–93.
39. Saunders L, Ouellette A, Bandle R, et al. Identification of small-molecule inhibitors of autotaxin that inhibit melanoma cell migration and invasion. Mol Cancer Ther 2008;7:3352–62.
40. Hama K, Aoki J, Fukaya M, et al. Lysophosphatidic acid and autotaxin stimulate cell motility of neoplastic and non-neoplastic cells through LPA1. J Biol Chem 2004;279:17634–9.
41. Aoki J, Inoue A, Okudaira S. Two pathways for lysophosphatidic acid production. Biochim Biophys Acta 2008;1781:513–8.
42. van Meeteren L, Moolenaar W. Regulation and biological activities of the autotaxin-LPA axis. Prog Lipid Res 2007;46:145–60.
43. Fleming IN, Elliott CM, Collard JG, Exton JH. Lysophosphatidic acid induces threonine phosphorylation of Tiam1 in Swiss 3T3 fibroblasts via activation of protein kinase C. J Biol Chem 1997;272:33105–10.
44. Gschwind A, Prenzel N, Ullrich A. Lysophosphatidic acid-induced squamous cell carcinoma cell proliferation and motility involves epidermal growth factor receptor signal transactivation. Cancer Res 2002;62:6329–36.
45. Nam S, Clair T, Kim Y-S, et al. Autotaxin (NPP-2), a metastasis-enhancing motogen, is an angiogenic factor. Cancer Res 2001;61:6938–44.
46. Federico L, Pamuklar Z, Smyth S, Morris A. Therapeutic potential of autotaxin/lysophospholipase D inhibitors. Curr Drug Targets 2008;9:698–708.
47. Scaife CL, Shea JE, Dai Q, Firpo MA, Prestwich GD, Mulvihill SJ. Synthetic extracellular matrix enhances tumor growth and metastasis in an orthotopic mouse model of pancreatic adenocarcinoma. J Gastrointest Surg 2008;12:1074–80.
48. van Meeteren LA, Ruurs P, Stortelers C, et al. Autotaxin, a secreted lysophospholipase D, is essential for blood vessel formation during development. Mol Cell Biol 2006;26:5015–22.
49. Apsel B, Blair J, Gonzalez B, et al. Targeted polypharmacology: discovery of dual inhibitors of tyrosine and phosphoinositide kinases. Nat Chem Biol 2008;4:691–9.